

# Monolithic 3D printed waveguide filters with wide spurious-free stopbands using dimpled spherical resonators

Guo, Cheng; Yu, Yang; Li, Sheng; Wen, Xiaozhu; Zhang, Anxue; Wang, Yi; Attallah, Moataz

DOI:  
[10.1049/mia2.12178](https://doi.org/10.1049/mia2.12178)

License:  
Creative Commons: Attribution-NonCommercial-NoDerivs (CC BY-NC-ND)

Document Version  
Publisher's PDF, also known as Version of record

Citation for published version (Harvard):  
Guo, C, Yu, Y, Li, S, Wen, X, Zhang, A, Wang, Y & Attallah, M 2021, 'Monolithic 3D printed waveguide filters with wide spurious-free stopbands using dimpled spherical resonators', *IET Microwaves, Antennas and Propagation*, vol. 15, no. 12, pp. 1657-1670. <https://doi.org/10.1049/mia2.12178>

[Link to publication on Research at Birmingham portal](#)

## General rights

Unless a licence is specified above, all rights (including copyright and moral rights) in this document are retained by the authors and/or the copyright holders. The express permission of the copyright holder must be obtained for any use of this material other than for purposes permitted by law.

- Users may freely distribute the URL that is used to identify this publication.
- Users may download and/or print one copy of the publication from the University of Birmingham research portal for the purpose of private study or non-commercial research.
- User may use extracts from the document in line with the concept of 'fair dealing' under the Copyright, Designs and Patents Act 1988 (?)
- Users may not further distribute the material nor use it for the purposes of commercial gain.

Where a licence is displayed above, please note the terms and conditions of the licence govern your use of this document.


When citing, please reference the published version.

## Take down policy

While the University of Birmingham exercises care and attention in making items available there are rare occasions when an item has been uploaded in error or has been deemed to be commercially or otherwise sensitive.

If you believe that this is the case for this document, please contact [UBIRA@lists.bham.ac.uk](mailto:UBIRA@lists.bham.ac.uk) providing details and we will remove access to the work immediately and investigate.

# Monolithic 3D printed waveguide filters with wide spurious-free stopbands using dimpled spherical resonators

Cheng Guo<sup>1,2</sup> | Yang Yu<sup>2,3</sup>  | Sheng Li<sup>4</sup> | Xiaozhu Wen<sup>1</sup> | Anxue Zhang<sup>1</sup> | Yi Wang<sup>2</sup> | Moataz Attallah<sup>4</sup>

<sup>1</sup>School of Information and Communication Engineering, Xi'an Jiaotong University, Xi'an, Shaanxi, China

<sup>2</sup>Department of Electronic, Electrical and Systems Engineering, University of Birmingham, Birmingham, UK

<sup>3</sup>Department of Electrical and Electronic Engineering, Southern University of Science and Technology, Shenzhen, China

<sup>4</sup>School of Metallurgy and Materials, University of Birmingham, Birmingham, UK

## Correspondence

Yang Yu, Department of Electrical and Electronic Engineering, Southern University of Science and Technology, Shenzhen, 518055, China.  
Email: [issacyu@live.cn](mailto:issacyu@live.cn)

## Funding information

National Natural Science Foundation of China, Grant/Award Number: 62001367

## Abstract

Employing a family of dimpled and slotted spherical resonators, and a set of X-band waveguide bandpass filters (BPFs) is presented in this study. The resonators originated from spherical resonators with depression (hence, dimples are formed) and cutting slots into the resonator shell. With a large number of experiments, the combination of using the twisted coupling topology, depression and slotting on the resonators results in filters with simultaneous low insertion loss (IL), good out-of-band rejection and wide spurious-free stopband. Several BPFs are designed and 3D printed using the selective laser melting (SLM) technique where they are made in one piece. The monolithic implementation of these filters is allowed by the compatibility of the microwave and the mechanical design, which minimises the required supporting structures inside the filters. The measurement results show ILs of 0.2–0.3 dB and are better than 15 dB return loss. There is a small frequency shift of less than 0.9%, and a measured spurious-free stopband covering the entire X–Ku bands (8.2–18 GHz) with rejection over 34 dB. Additionally, for the SLM printed devices, the influences of temperature to the S-parameter responses, as well as polishing, which lowers the losses, are included in this study.

## 1 | INTRODUCTION

Air-filled metallic cavity resonators are fundamental units for microwave and millimetre-wave devices and applications [1]. Example devices include waveguide filters [2], multiplexers [3–5], filtering antennas [6, 7], Butler matrices [8] and impedance matching networks for semiconductor devices [9, 10]. High unloaded quality factor ( $Q_u$ ) resonators are usually preferred to minimise the total loss of these devices. The  $Q_u$  of an air-filled metallic cavity resonator is mainly determined by the cavity geometry, the electrical conductivity and to a lesser extent to the surface roughness [11, 12]. Spherical cavity resonator exhibits the highest  $Q_u$  of dominant mode among all

possible three-dimensional geometries (e.g. rectangular and cylindrical cavity), due to its highest volume-to-surface-area ratio [13]. The  $Q_u$  of a spherical cavity is calculated to be around 1.8 times than that of a rectangular one at the same working frequency. Recently, the rapid development of additive manufacturing (AM) technology [14] has enabled the realisation of geometrically sophisticated waveguide devices. Some examples are the X-band waveguide filters based on single-/multi-mode spherical resonators [15–20]. Such filters have provided a very low insertion loss (IL). However, one drawback is that the spherical resonator suffers from spurious modes closer to the fundamental mode compared with the rectangular resonator. This is undesired where high out-of-

This is an open access article under the terms of the Creative Commons Attribution-NonCommercial-NoDerivs License, which permits use and distribution in any medium, provided the original work is properly cited, the use is non-commercial and no modifications or adaptations are made.

© 2021 The Authors. *IET Microwaves, Antennas & Propagation* published by John Wiley & Sons Ltd on behalf of The Institution of Engineering and Technology.

band rejection and wide spurious-free stopbands are of critical concern for the application.

Several studies have focussed on the above-mentioned problem. In our previous work, a 90°-twisted inter-resonator coupling geometry was proposed to reduce the propagation of the higher-order modes [15]. By doing so, the out-of-band rejection was significantly improved as compared with that of an inline configuration. Another effective approach for extending spurious-free stopbands is to physically alter the geometry of a single cavity to tune the higher-order modes farther away from the dominant mode. Care must of course be taken not to reduce the unloaded quality factor of the dominant mode too much. Examples of this geometrical redesign of the resonators are given in [21, 22]. The results show that the eigenmode frequency of the first higher-order mode increases by 27% as compared with that for a rectangular resonator, and simultaneously with a 13% improvement for the  $Q_u$ . Despite that [21, 22] were comparing their results with the rectangular resonators, the principles are the same and the result is very appealing in filter applications, but tradeoffs do exist between the two critical factors of  $Q_u$  and spurious-free bandwidth. Another interesting approach is to radiate the unwanted modes by putting slots on a spherical resonator [23]. The slots are in parallel with the fundamental mode currents, but perpendicular to some of the spurious mode currents. However, the approach has a drawback in that the filter becomes strongly radiative in its stopband. Similar to the spherical resonator work in [23], a slotted hemispherical resonator was used to address the same issue in [24]. When compared with the filter in [23], the slotted hemispherical filter is much less radiative. However, the  $Q_u$  for the hemispherical resonator is almost the same as the rectangular resonator; hence the advantages of this complex geometry become less obvious.

This study investigates bandpass filters (BPFs) with simultaneous low loss, wide spurious-free stopband and good out-of-band rejection based on a family of dimpled and slotted spherical resonators, as well as their AM. The innovative design approaches are as follows: (1) depress the spherical cavities to tune the higher-order mode further away from the fundamental mode; (2) appropriately opening slots on the resonator shells that are non-radiative for the fundamental mode and radiative for the undesired higher-order modes; (3) employing unequal sized dimples in spherical resonators in the filters to detune the spurious passbands; (4) arranging the aforementioned resonators in a 90°-twisted coupling configuration to minimise the inter-resonator coupling for the higher-order modes; (5) locate the different dimpled resonators according to the  $g$  values in the low-pass filter prototype to minimise the loss. Approach (1) is similar to the method reported in [21, 22], and it sacrifices the  $Q_u$  of the spherical resonator for an extended spurious-free stopband (still much higher than the conventionally used rectangular resonators). Approach (2) removes one or a few higher-order modes without degrading the  $Q_u$  of the fundamental mode at the expense of generating strong radiation at stopbands. Approach (3) and (4) contribute to the stopband extension and significantly reduce the unwanted radiation for a

wide frequency range caused by slotting. Approach (5) gives an idea of how the unequally dimpled resonators should be arranged for maximum effectiveness within the filter. It should be mentioned that if either the innovation were used individually, the performance of the filter would improve (e.g. [15, 21–23]) but not be optimal. In this study, a design that integrates all the five approaches is proposed. Interestingly, by doing so, the trade-off between the  $Q_u$  and the spurious-free bandwidth can be alleviated.

Considering the geometric complexity of the devices, 3D printing was used for effective construction. The 3D printing technique used was selective laser melting (SLM) enabling the monolithic manufacturing of these filters by avoiding any assembly. This is possible as the filters are designed to be compatible with the fabrication process with, for example, minimal internal supporting structures.

The content of this study is organised as follows. The theory, structural design and characterisation of the dimpled and slotted spherical resonators are described in Section 2. These types of resonators were presented in [25], but we include a short review here for completeness. Furthermore, some thermal consideration is also included in this section. Then, the design, implementation and measurements for the BPFs are discussed in Section 3. Finally, Section 4 concludes the study.

## 2 | REVIEW OF THE DIMPLED AND SLOTTED SPHERICAL RESONATORS AND THEIR THERMAL CONSIDERATIONS

In this section, we include a short review of the results presented in [25] (part A–part C). The thermal considerations, as well as surface roughness measurement, will be presented in Sections 2.4 and 2.5.

### 2.1 | Dimpled resonators

As shown in Figure 1, the first higher-order mode transverse magnetic ( $TM_{201}$ ) in a spherical resonator can be tuned farther away from the fundamental  $TM_{101}$  mode by the dimple the cavity. As shown in Figure 1, by varying the depth  $d$  of the intersection, a group of dimpled spherical resonators can be constructed. As the cavity is progressively dimpled, the  $Q_u$  becomes lower. However, during this the resonant frequency of the first higher-order mode increases. Figure 2 shows the  $S_{21}$  for the four resonators in Figure 1b–e, using two ports and weak coupling. While the resonant frequencies and  $Q_u$  of the modes of interest are summarised in Table 1. These results show the extension of the stopband bandwidth at the expense of degraded fundamental-mode  $Q_u$ . Therefore, for practical filter applications, an appropriate group of parameters for the dimpled cavities needs to be selected as a compromise between the passband IL and the spurious-free stopband bandwidth.

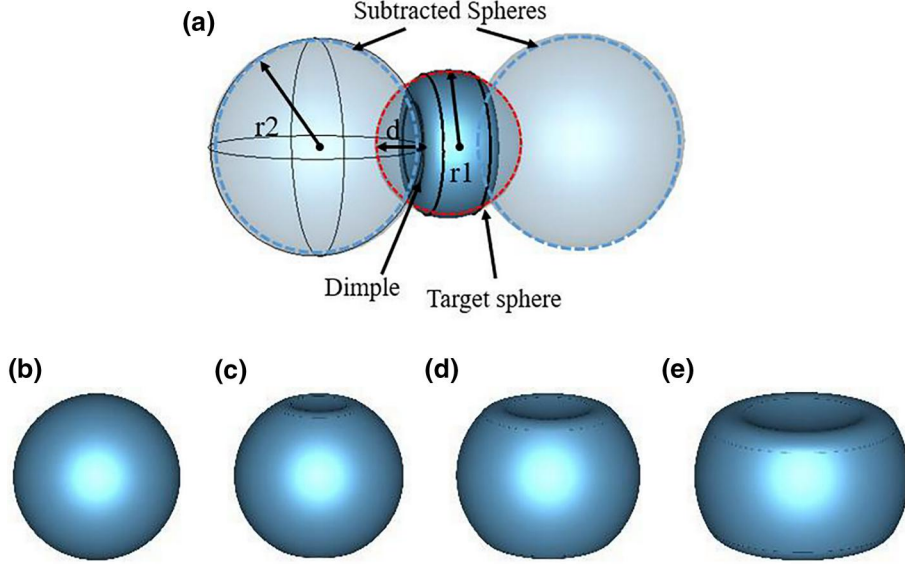


**FIGURE 1** Geometrical shaping of an air-filled spherical resonator. (a) The simulation model with critical dimensions showing the principle of shaping; (b) A conventional spherical resonator ( $r_1 = 13.1$ ,  $d = 0$ ); (c) A slightly dimpled resonator ( $r_1 = 12.925$ ,  $d = 2$ ); (d) A moderately dimpled resonator ( $r_1 = 12.417$ ,  $d = 4$ ); (e) A highly dimpled resonator ( $r_1 = 11.67$ ,  $d = 6$ ). The radius  $r_2 = 17.5$  is used for all the dimpled resonators. All the above cavity dimensions are in millimetres and are selected for a dominant-mode resonance at 10 GHz

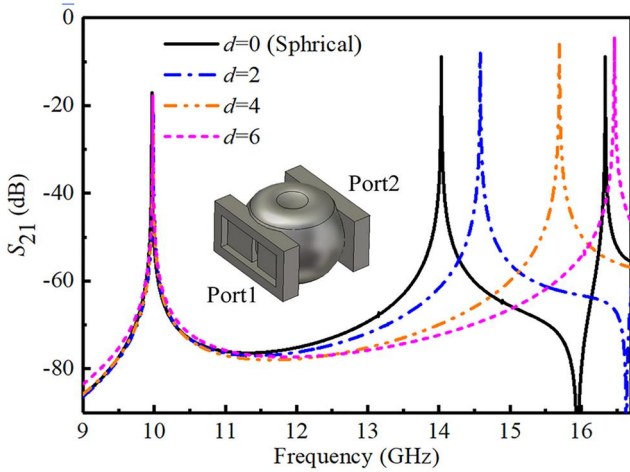


**FIGURE 2** Simulated  $S$ -parameter response of a two-port weak-fed spherical resonator with geometrical shaping. The inset illustrates the simulation model of the dimpled spherical resonator. Feeding windows of  $3.43 \times 10.16$  mm were used (and been used in the fabrication model)

## 2.2 | Slotting on cavity shells

Although the stopband bandwidth can be improved by a dimple in the resonator, the higher order mode in the resonator cannot be removed. An effective approach to remove the higher-order mode is by slotting the cavity shell [23–26]. In Figure 3, the simulated surface current distribution for the fundamental is illustrated and first higher-order mode in the dimpled resonator shown in Figure 1d. As it can be seen, in the dimpled areas on the top, the surface current reaches the minimum for the fundamental mode but is maximum for the first higher-order

**TABLE 1** Comparison of several types of cavity resonators at 10 GHz

Resonators	$Q_u/Q_{Rec}$	Dimensions (mm)	1st higher order mode freq (GHz)
Rectangular	1	$22.86 \times 10.16 \times 19.9$	15.1
Figure 1b	1.816	$r_1 = 13.1, d = 0$	14.1
Figure 1c	1.734	$r_1 = 12.925, d = 2$	14.5
Figure 1d	1.533	$r_1 = 12.417, d = 4$	15.6
Figure 1e	1.243	$r_1 = 11.670, d = 6$	16.4

Note:  $Q_{Rec}$ , The dominant-mode  $Q_u$  of a rectangular waveguide resonator.  $Q_{Rec} = 4566$  at 10 GHz for lossy ( $\sigma = 1.9 \times 10^7$  S/m) boundaries with zero surface roughness.

mode. If a slot is opened along a direction that is perpendicular to the surface current of the first higher-order mode (in the meantime, parallel to that of the fundamental-mode current), the first higher-order mode can be removed by radiation without affecting the fundamental mode. Figure 4a shows the resonator with this single slot.

However, like many other TM mode resonators, the first higher-order mode is degenerated in two orthogonal orientations [27]. To take the mode degeneracy into account, a cross-slot can be used as shown in Figure 4b. The cross slot is equivalent to a single rectangular slot for cutting the surface current from any orientation of polarisation. This will be very useful when non-inline filter topology is used, so the degenerate mode can also be excited (and can only be removed by the cross slot), such as the filters presented in the following sections.

Figure 5 shows the simulated  $S_{21}$  for a two-port weakly coupled dimpled spherical resonator before and after slotting

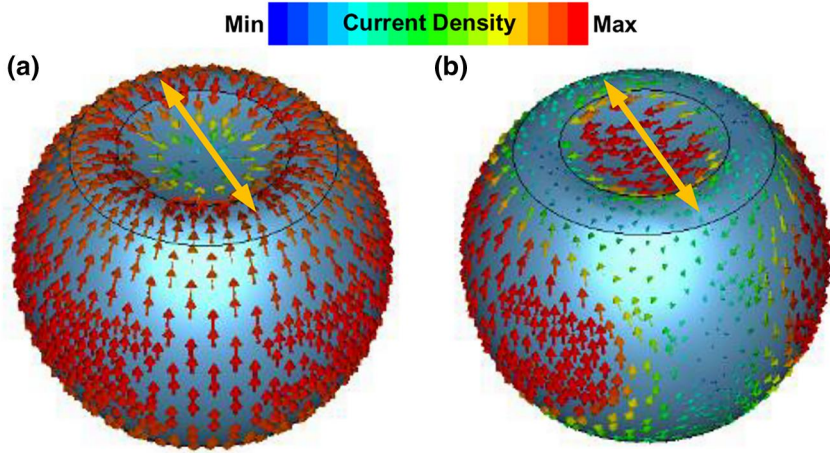


**FIGURE 3** Simulated surface current distribution for a symmetrically dimpled spherical resonator. The yellow arrow represents a possible slotting orientation. (a) The fundamental-mode at 10 GHz. The slotting orientation is parallel to that of the surface current in the dimpled area; (b) The first higher order mode at 15.6 GHz. The slotting orientation is perpendicular to that of the surface current in the dimpled area

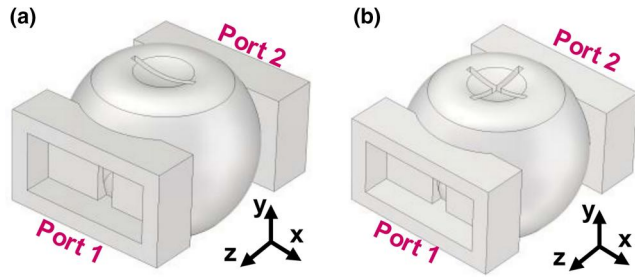


**FIGURE 4** The two-port weakly fed simulation models of the proposed slotted and dimpled spherical resonators. (a) A 3D view of the rectangular-slotted resonator; (b) A 3D view of the cross slotted resonator

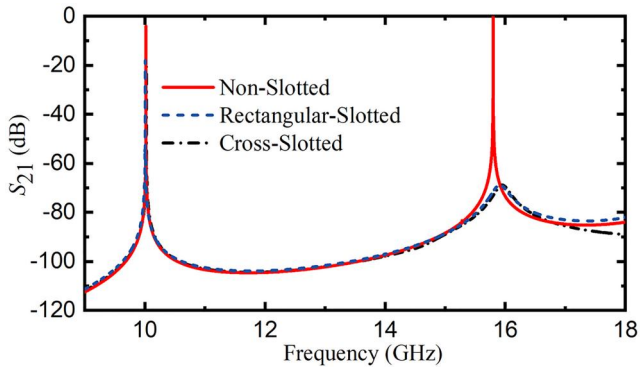


**FIGURE 5** Comparison in the simulated  $S$ -parameter response of a two-port weakly coupled shaped spherical resonator before and after slotting the cavity shell

the cavity shell. As it can be seen, with either a rectangular or cross slot, the first higher-order mode at around 16 GHz is removed without affecting the fundamental mode. To quantify the effect of slotting on these two modes, the radiation quality factor ( $Q_r$ ) can be evaluated and listed in Table 2, the detailed calculations can be found in [25, 28]. As it can be seen, the  $Q_r$  for the fundamental mode is  $5 \times 10^5$  (for the cross slot) and  $2 \times 10^6$  (for the single slot), which is about 2 orders of magnitude higher than  $Q_c$ , whereas the  $Q_r$  for the first higher order mode is only 60–70. This indicates that the slots have

**TABLE 2** Calculated radiation  $Q_s$  for different slot geometries

Slot geometries	Slot dimensions (mm)	$Q_{r1}$	$Q_{r2}$
Rectangular	$16 \times 1.5$ mm	$2.1 \times 10^6$	67.6
Cross	$16 \times 1.5$ mm (each)	$5.5 \times 10^5$	62.4

Note:  $Q_{r1}$  and  $Q_{r2}$ , The radiation  $Q$  for the fundamental mode and the first higher order mode, respectively. The  $Q_r$  were obtained using PEC boundaries for the cavity resonators with feeding windows of  $2.28 \times 10.16$  mm. Note that the size of the feeding windows is different from the one in Figure 2, this is to ensure the calculation is with high accuracy ( $Q_c$  approaching infinity).

little interference on the fundamental mode while the unwanted mode is radiated out. The length and width of the slots were chosen to realise enough suppression without dramatically degrading the fundamental mode  $Q_u$ .

For the selected dimensions in Table 2, the  $Q_u$  of the resonators with non-slot, a rectangular-slot and a cross-slot operating at fundamental-mode are 6850, 6820 and 6800, respectively, using an aluminium alloy with the electrical conductivity of  $1.9 \times 10^7$  S/m [29]. The difference in the calculated  $Q_u$  mainly comes from the slight variation in the cavity volume.

### 2.3 | Fabrication and microwave characterisation

A non-slotted resonator and a single-slotted resonator were fabricated using a metallic SLM technique [25]. Figure 6 shows the SLM-printed resonators.

The resonators were measured using a Keysight network analyser (E8362C), and the frequency responses at X and Ku bands were measured individually. For the measurement of the Ku-band response, a pair of X-to-Ku-band waveguide tapers were used. Figure 7 compares the simulated and measured results, showing good agreement. The measured frequency shifts for the fundamental mode are about 0.8%. They are caused by the volume shrinkage during printing and can be further reduced by a structural compensation [30–32]. It is shown in Figure 7 that for the slotted resonator, the first higher-order mode at 15.8 GHz is removed. The  $Q_u$  extracted

**FIGURE 6** Photographs of the metallic selective laser melting-printed X-band dimpled spherical resonators. (a) The non-slotted resonator; (b) The rectangular-slotted resonator

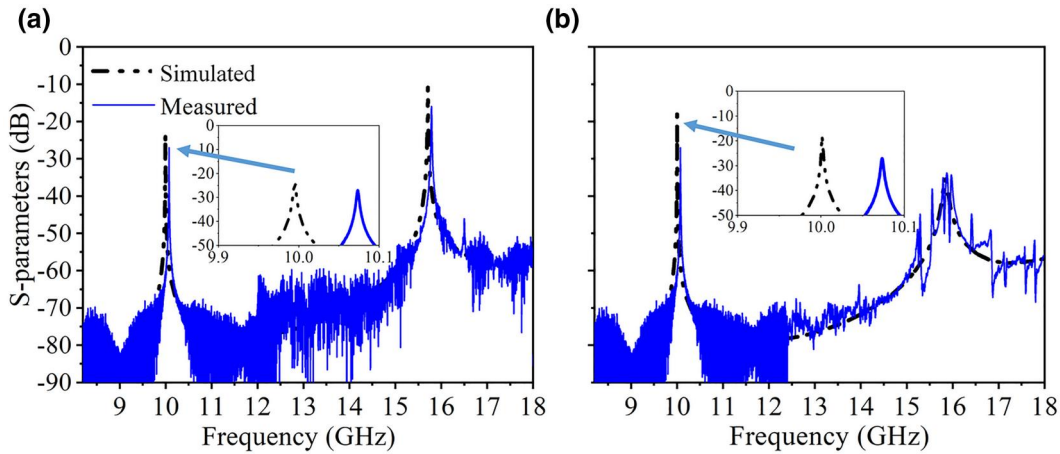
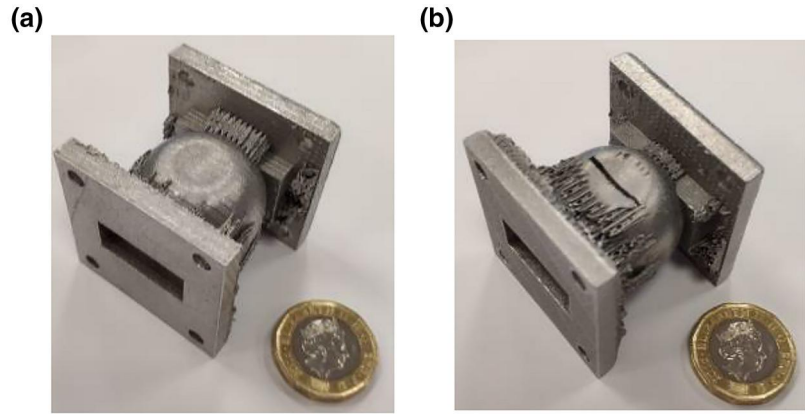


**FIGURE 7** Simulated and measured wideband (X-to-Ku-band)  $S$ -parameter responses of the X-band symmetrically squeezed spherical resonators. (a) The non-slotted resonator; (b) The rectangular-slotted resonator

from the measured  $S_{21}$  are 3608 and 3377 for the non-slotted and rectangular-slotted resonators, respectively.

The difference between the simulated and measured  $Q_u$  can be attributed to the non-zero surface roughness, as we have already used the conductivity of the Al alloy. This can be improved through a post polishing process detailed in [25]. The effective electrical conductivity of the printed aluminium alloy could be improved by reducing the surface roughness. As a result, the simulated and measured  $Q_u$  before and after polishing for the resonators are compared in Table 3. As it can be seen, the  $Q_u$  can be improved by about 20% during the process. To consider the discrepancies between the simulation and experiment, an effective conductivity of about  $8 \times 10^6$  S/m for the aluminium alloy was used in CST to match the re-simulated  $Q_u$  to the measured values, this will be used in the filter design.

## 2.4 | Thermal capabilities

An experiment was conducted further on characterising the thermal capabilities of the SLM printed resonator. This is necessary as the 3D printed devices may not be perfectly solid and the thermal expansion coefficient (C.T.E) may differ from the fully condensed parts. The measurement setup described in

**TABLE 3** Simulated and measured  $Q$  before and after polishing

Cavity	$Q_u$ (Sim.)	$Q_u$ (Meas.)	$Q_u$ (Pol.)
No slot	6854	3608	4328
With slot	6820	3377	3966

[17] was directly used. The  $S_{21}$  of the slotted resonator was measured for temperatures up to  $140^\circ\text{C}$  in a ramp-up and ramp-down cycle. The measured results plotted in Figure 8 show that the resonant frequency is decreased by about 0.23% (23 MHz) at  $140^\circ\text{C}$  as compared with the one at the room temperature of about  $25^\circ\text{C}$ . This corresponds to a linear frequency change of about 0.2 MHz/ $^\circ\text{C}$ . This frequency change corresponds to a C.T.E of about  $20 \times 10^{-6}/\text{K}$  for the utilised aluminium alloy and is consistent with the C.T.E of the alloy in the reference [29], which is  $22.5 \times 10^{-6}/\text{K}$ .

## 2.5 | Surface roughness measurements

The surface morphology for the SLM printed resonators was characterised by incorporating surface roughness testing [33] and scanning electron microscopy. The purpose of doing this is

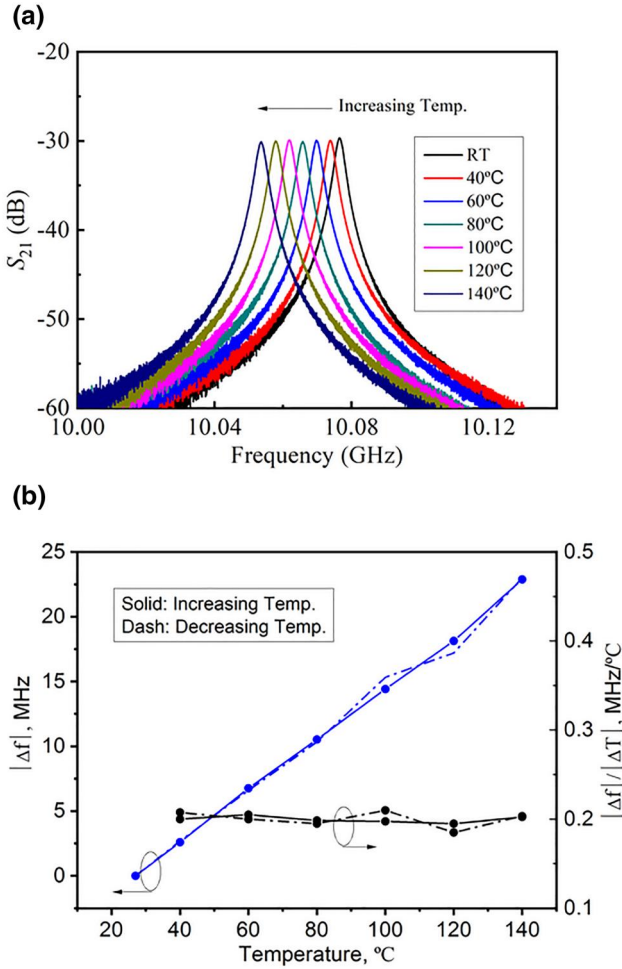


**FIGURE 8** Characterisation of the thermal handling capability for the resonator. (a) The measured  $S$ -parameter responses under different temperatures; (b) The extracted absolute resonant frequency drift and drift rate. RT, room temperature

not to use the data in re-simulation (because the surface quality can be very different at different locations) but to understand the SLM process itself better, so the device can be better designed based on the characteristics of the process. Considered that the resonators are too large for the measurement equipment, some printed  $2 \times 2 \times 0.5 \text{ cm}^3$  samples with different printing orientations were used. Figure 9 shows how these samples were printed. The measured roughness (Ra) before and after polishing are listed in Table 4. Note that for the downward face, the roughness is much higher (10 $\times$ ) than the others, because it requires lots of supporting structures during the printing process. These supporting structures are attached to the downward face and can be difficult to be removed by post processing. Note that for the 45 $^\circ$  downward face, less support is needed which is mostly distributed at the edges of the structure. Figure 10 shows the images for the upward and downward faces. As it can be seen, the quality of the downward face is very poor.

As a conclusion, in the filter design, such downward faces need to be avoided by properly designing the filter structure as

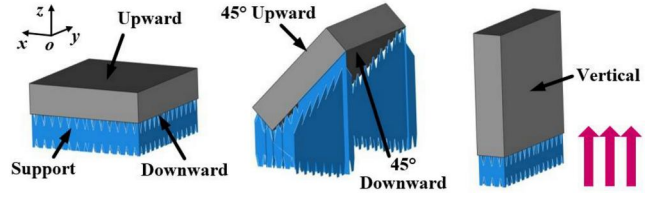


**FIGURE 9** Samples with different printing orientations. For the 45 $^\circ$  structure, the supports at the upper edge is hidden

**TABLE 4** Surface roughness before and after polishing

	Upward	Downward	45 $^\circ$ up	45 $^\circ$ down	Vertical
Before	3.1	34	4.1	6.4	4.8
After	2.5	24.1	3.4	3.3	2.8

Note: Dimensions in  $\mu\text{m}$ .

well as properly choosing the printing orientation; this will be discussed in Section 3.

### 3 | DESIGN, FABRICATION AND CHARACTERISATION OF FILTER PROTOTYPES

The proposed resonators are used in a set of filters; all of them were designed with a centre frequency of 10 GHz, a fractional bandwidth of 5%, a return loss (RL) of 20 dB and a filter order of 5. The corresponding denormalised non-zero external and inter-resonator coupling coefficients are  $M_{S1} = M_{5L} = 0.0507$ ,  $M_{12} = M_{45} = 0.0433$  and  $M_{23} = M_{34} = 0.0318$  [28]. A series of designs to demonstrate the principles mentioned in the introduction will be progressively described in the following content for the realisation of BPFs with low-loss passbands and wide spurious-free stopbands. Note that this study mainly focusses more on appropriately adding slots on the dimpled spherical resonators to improve the filter performance. However, it is possible to make the filter responses more complex, for example transmission zeros. To realise this, either the cross-couplings or extracted pole topology can be adopted. Moreover, the multi-mode characteristics of the spherical resonators can be utilised to realise the filtering responses with transmission zeros. With the multi-mode operations, the designed filter will be more compact and low loss. Some the state-of-the-art investigations have already demonstrated this point [16, 34].

#### 3.1 | Design A (equal size dimpled resonators in twisted coupling topology)

Using the dimpled resonator, a group of filters can be designed based on the 90 $^\circ$ -twisted coupling topology reported in [15]. The twisted coupling topology will be used in all the filters and is seen in Figures 11–13. Figure 11 shows the simulation results for a group of filters (Filter D1 to Filter D4, ‘D’ is for

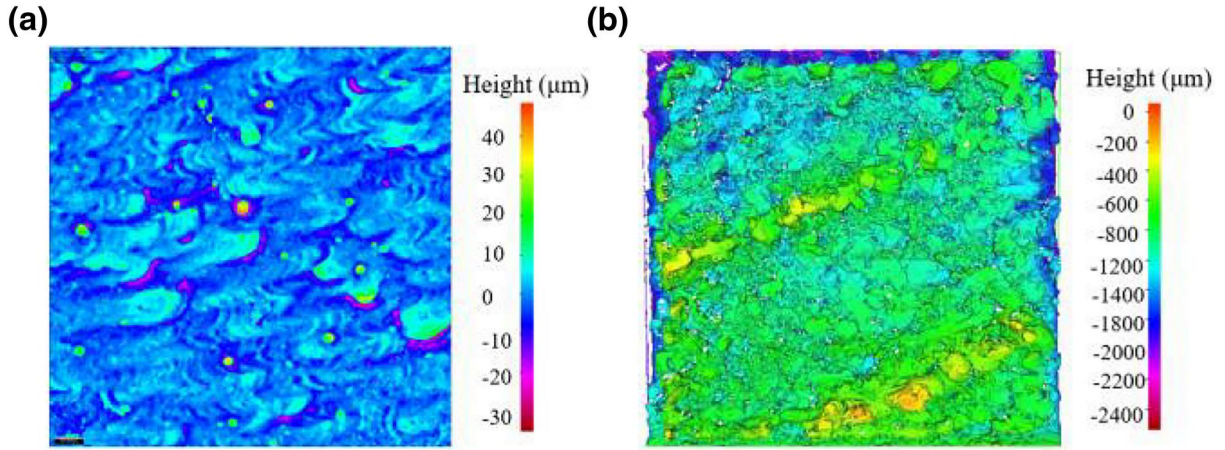


**FIGURE 10** Photographs for the upward and downward faces. (a) upward face; (b) downward face. The absolute value of the height is arbitrary and only depends on the focussing plane during imaging

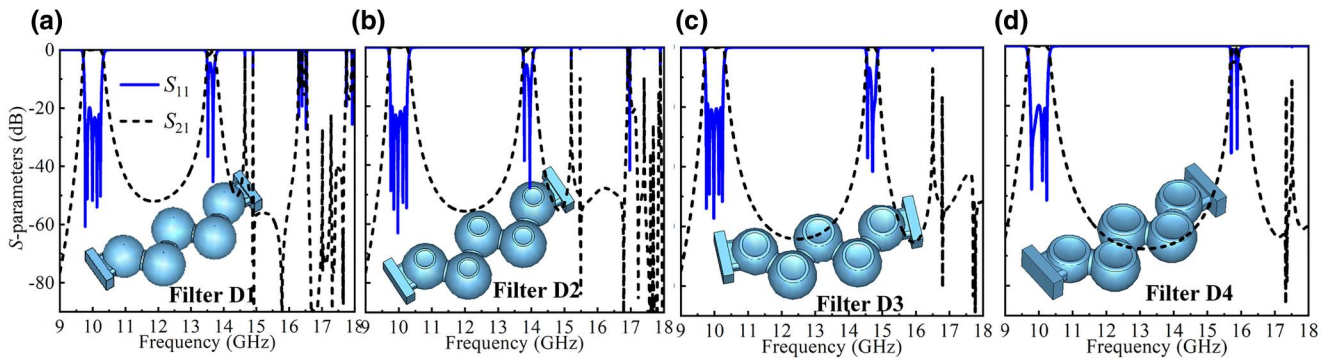


**FIGURE 11** Simulation results for a group of filters based on a sequence of constant dimpled resonators. (a) based on spherical resonator ( $d = 0$ ); (b) based on slightly dimpled resonator ( $d = 2$ ); (c) based on moderately dimpled resonator ( $d = 4$ ); (d) based on heavily dimpled resonator ( $d = 6$ )

‘Dimple’), each filter has equal-sized dimples in its resonators as defined in Figure 1a–d. For each filter, all the resonators are dimpled by the same amount (we will discuss filters with unequal-sized dimples later). As expected, the more the resonators are dimpled, the better rejection can be obtained. For example, many spurious passbands exist in Filter D1 where the first one appears at around 13.6 GHz, whilst the first spurious passband appears at 16 GHz for Filter D4. This is similar to the works presented in [21, 22], however, the latter only uses in-line coupling topology in the filter design.

### 3.2 | Design B (slotted resonators in twisted coupling topology)

As mentioned in Section 2 and also demonstrated in [23, 24], another effective way of removing the higher-order mode is to slot the resonators. Hence, in this section, slotted resonators are used to design a group of filters. First of all, in order to know the relationship between filter performance and the number of slots. Three filters were designed (Filter S1–S3, ‘S’ is for ‘Slotted’), as shown in Figure 12a–c. In general, when one to five cross slots were placed on the spherical resonators, the

stopband rejection until 18 GHz is from  $>9$  dB to  $>23$  dB, respectively. Note that, as the twisted coupling topology is used in the design, the rectangular slot cannot effectively remove the higher-order modes, as discussed in Section 2 (due to the polarisation degeneracy). For example, Figure 12d shows a filter with five rectangular slots and the performance is no better than the filter with a single cross slot shown in Figure 12a.

Especially, for filter S3, with cross slots in all the resonators, a wide stopband (rejection better than 20 dB) up to 18 GHz is formed. However, it also becomes heavily radiative for a wide frequency range as the  $S_{11}$  is also lower than  $-10$  dB over 13 GHz. This happens because, as shown in Table 2, the radiation  $Q$  of the slotted resonator's first higher-order mode is only 50–60. To quantify the radiation, the corresponding total radiation efficiencies (defined as the ratio in dB between the radiated power and the input power) are simulated for 10 GHz (passband) and frequencies 13.49, 14.41, 17.66 GHz ( $S_{11}$  minimums at the stopband). The results are  $-25.84$ ,  $-0.04$ ,  $-0.01$  and  $-0.11$  dB, respectively. As expected, this indicates negligible radiation in the passband and strong radiation in the stopband. The radiation in the stopband could interfere with the external circuits in the system. This can be alleviated by placing an absorber over the slots.



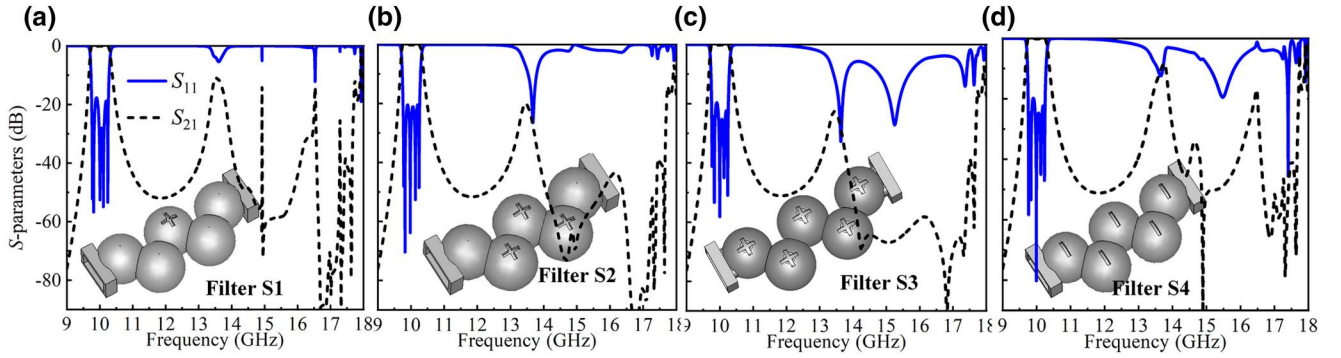


**FIGURE 12** Simulation results for a group of filters based on slotted spherical resonators. (a) with one cross slot, (b) with three cross slots, (c) with five cross slots, (d) with five rectangular slots. All the slots are with dimensions of  $10 \times 2$  mm

### 3.3 | Design C (combination of the slotted and equally dimpled resonators)

From the previous discussions, we know that the stopband performance can be improved by either dimpling the resonators heavier or by slotting more resonators in the filter. Now, it is natural to consider combining the two methods together. For the first attempt, we combine Filter D2 and S2 together (to put three cross slots on Filter D2), the new filter is called Filter DS1 (‘DS’ for ‘Dimpled and Slotted’).

The filter is shown in Figure 13a together with its simulation results. Interestingly, on one hand, Filter DS1 provides a rejection of  $>30$  dB until 18 GHz, which is much better than that of the filters D3 (heavily dimpled) and S3 (all slotted). On the other hand, its radiation performance is similar to that of Filter S2.

Apparently, by doing a combination, more filters like three slots on Filter D3, five slots on Filter D3 or even five slots on Filter D4 can be designed and trivially they will have better stopband performances compared with Filter DS1. We are not interested in them as they sacrifice the  $Q_u$  a lot more and simultaneously introduce more unwanted radiation in the stopband. Instead, we wish to find a possible solution in which most of the merits (low loss, wide stopband and low radiation) can be preserved. To understand how this can be achieved, another three filters are designed by putting only one cross slot on Filter D2–D4, the simulation results are plotted in Figure 13b–d. Now, we can look at Filter S1, Filter DS2–DS4 as a new group and compare them with the Filters D1–D4. It can be observed in the following that: (i) the radiation always appears at the positions of the spurious passband of the original (non-slotted) filter. (ii) if we compare Filter S1 and DS4, it can be found that Filter DS4 got more rejection and less radiation than Filter S1. This is quite different from the cases when three to five slots are added (the better the rejection, the stronger the radiation, see Filter S3 and Figure 12c).

Considering the facts described above, we believe the more appropriate strategy for combining the dimpled and slotted resonators is given as follows: (i) to create a wide (but no need to be deep) stopband while trying to keep the high  $Q_u$  properties of the resonators. (ii) one slot can be placed on the filter

to improve the rejection performance without introducing strong radiation in the stopband. This design philosophy will be demonstrated in the next 2 sections, with the addition of unequal dimple sizes in any one filter.

### 3.4 | Design D (unequally dimpled and selectively slotted resonators)

Following the design philosophy discussed above, a filter (Filter UD1, ‘UD’ is for ‘Unequally Dimpled’) with a wide stopband is proposed. In this design, the resonators are unequally dimpled by introducing different  $d$  and  $r_2$  values (see Figure 1). Under such a circumstance, the resonators can be tuned to exhibit the same fundamental-mode frequency but different higher-order mode frequencies (see Figure 2). Hence, the spurious passbands can be intentionally detuned when combined into the final filter. The Filter UD1 is illustrated in Figure 14. The design flow of this filter is summarised as follows: First, five resonators were designed individually. The intersection depths of  $d = 2, 4$  and  $6$  mm were used for these resonators. Then, the highly dimpled ( $d = 6$  mm) resonator was placed in the middle (resonator 3) to maximise the detuning. The three moderately dimpled ( $d = 4$  mm) resonators were used for resonators 1, 2 and 4, whereas the slightly dimpled ( $d = 2$  mm) resonator was utilised for resonator 5. Note that this is only one solution and many other arrangements for the resonators could be made flexible. Local multi-objective optimisation was carried out in CST for the passband and stopband, and the critical parameters (the parameters to be optimised) of the filter after optimisation are summarised in Figure 14.

The simulation results for Filter UD1 are shown in Figure 15a. It can be found that some spurious passbands still exist, but they were detuned to  $<-7$  dB until 18 GHz, demonstrating that the strategy of using the unequally dimpled resonators is quite effective. A cross slot can now be placed on resonator 3 to build a new filter called Filter UDS1 (‘UDS’ for ‘Unequally Dimpled and Slotted’). The simulation results for this filter can be found in Figure 15b, apparently, its performance is very appealing, as it provides rejection  $>37$  dB until

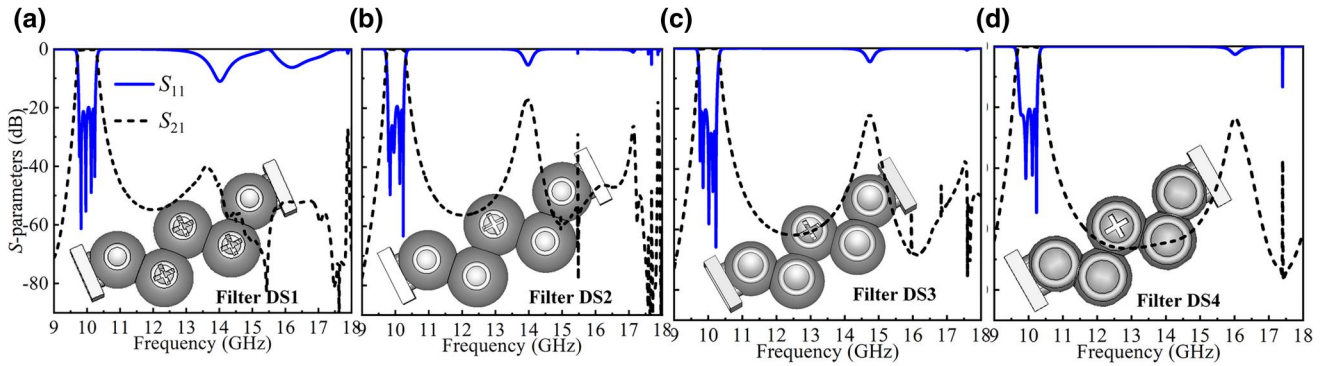


**FIGURE 13** Simulation results for a group of filters based on slotted and dimpled resonators. (a) with three cross slot and  $d = 2$ ; (b) with one cross slot and  $d = 2$ ; (c) with one cross slot and  $d = 4$ ; (d) with 1 cross slot and  $d = 6$

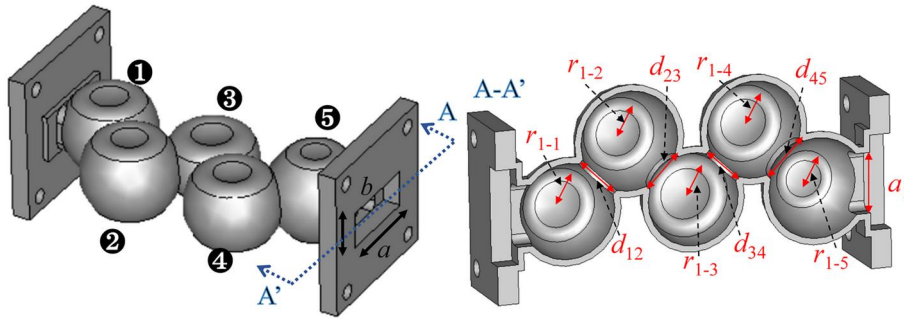
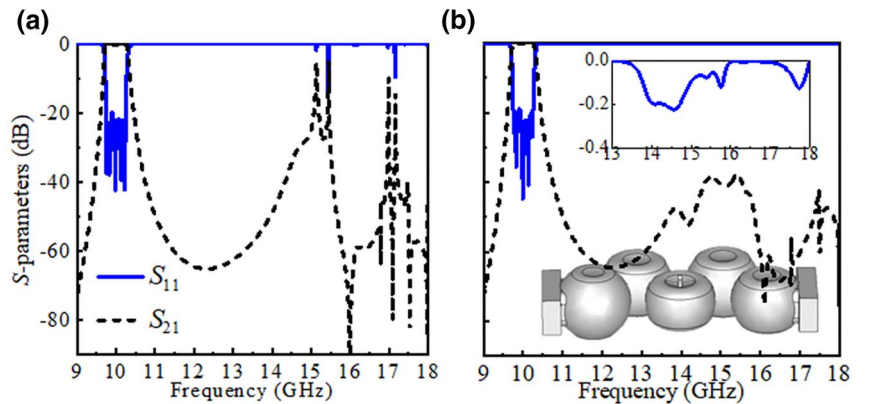


**FIGURE 14** A fabrication model of the Filter UD1. The critical dimensions are as follows:  $r_{1-1} = 11.489$ ,  $d_1 = 4.125$ ,  $r_{2-1} = 17.259$ ,  $r_{1-2} = 11.924$ ,  $d_2 = 4.080$ ,  $r_{2-2} = 14.35$ ,  $r_{1-3} = 11.129$ ,  $d_3 = 6.096$ ,  $r_{2-3} = 14.592$ ,  $r_{1-4} = 11.629$ ,  $d_4 = 4.740$ ,  $r_{2-4} = 13.546$ ,  $r_{1-5} = 12.088$ ,  $d_5 = 2.318$ ,  $r_{2-5} = 16.308$ ,  $a_1 = 14.576$ ,  $d_{12} = 11.515$ ,  $d_{23} = 10.325$ ,  $d_{34} = 10.141$ ,  $d_{45} = 11.739$ . The  $d_i$  and  $r_{2-i}$  ( $i = 1-5$ ) correspond to the intersection depth and the radius of the subtracted spheres for the  $i$ th resonator in Figure 14

**FIGURE 15** Simulation results for Filter UD1 and UDS1. (a) Filter UD1; (b) Filter UDS1, the insert shows the enlarged view of the  $S_{11}$  at the stopband



18 GHz and at the same time, very little radiation was generated ( $S_{11} > -0.2$  dB). Before we start to introduce any new designs, we can consider an experiment result of Filter UD1. It was fabricated with the same technique described in Section 2.3. During the fabrication, the  $45^\circ$ -tilted orientation, as illustrated in Figure 16a, was used to eliminate the use of too much internal support and to reduce the number of low-printing-quality downward faces. As discussed in Section 2, the surface quality of the SLM-printed downward faces (shown in Figure 10) can be much poorer than that of the upward or vertical faces.

With the orientation in Figure 16a, the downward faces of the resonators 3 and 5 were replaced by the coupling windows, as illustrated in Figure 16b, and were not printed. For comparison, Figure 17 shows some photographs of Filter UD1 which were printed using a different printing orientation. Obviously, the printing quality of the one shown in Figure 17a is much better than the one shown in Figure 17b, which was printed along with the narrow side of the input waveguide (with lots of downward faces).

Figure 18a shows the measured results for the filter shown in Figure 17b while Figure 18b–c shows the results for the filter

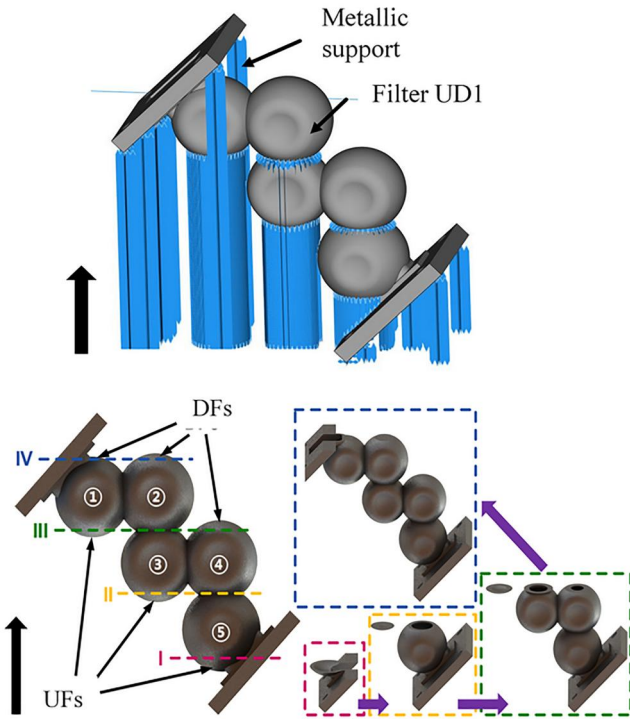


**FIGURE 16** The printing orientation for selective laser melting-printing the Filter UD1. (a) A schematic of the tilted posture showing generation of the supporting material; (b) An illustration presenting different phases I–IV of construction. DFs, downward faces; UFs, upward faces

shown in Figure 17a. Again, this demonstrates that the filter performance is highly dependent on the printing orientation. The good agreement between the simulation and measurement results demonstrates the high precision of the SLM process and the successfully chosen printing orientation. The fabricated filter has a passband RL better than 16 dB and an IL of about 0.2–0.3 dB. The shrinkage during manufacture causes the measured passband to shift about 0.86% towards higher frequencies.

### 3.5 | Design E (re-arranging the unequally dimpled resonators based on loss equations)

As discussed in the previous section, Filter UD1 was designed using local optimisation and some other arrangements for the resonators could be made. In this section, we attempt to demonstrate through an example (Filter UDS2) that if the slots are adopted, the arrangements of the unequally dimpled resonators can be better engineered, that is they can be arranged according to the  $g$  values of the corresponding lowpass prototype filter in order to minimise the IL without compromising the other performance. To understand this, the loss ( $\Delta L$ ) at the centre frequency of a filter that is designed from the lowpass prototype can be expressed as [28].

$$\Delta L = 4.343 \cdot \sum_{i=1}^n \frac{1}{\text{FBW} \cdot Q_{u-i}} g_i \text{ dB} \quad (1)$$

(a)



(b)

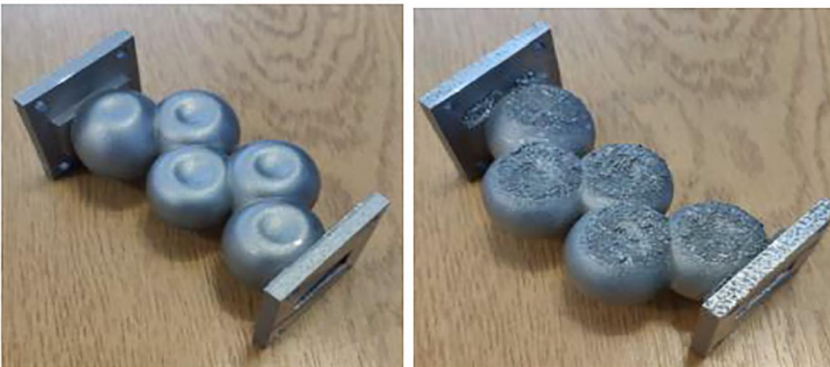


**FIGURE 17** Photographs of the selective laser melting-printed Filter UD1. (a) Using the printing orientation shown in Figure 16a; (b) Using a printing orientation in parallel with the narrow side of the input waveguide, the photos show the two faces of the same filter

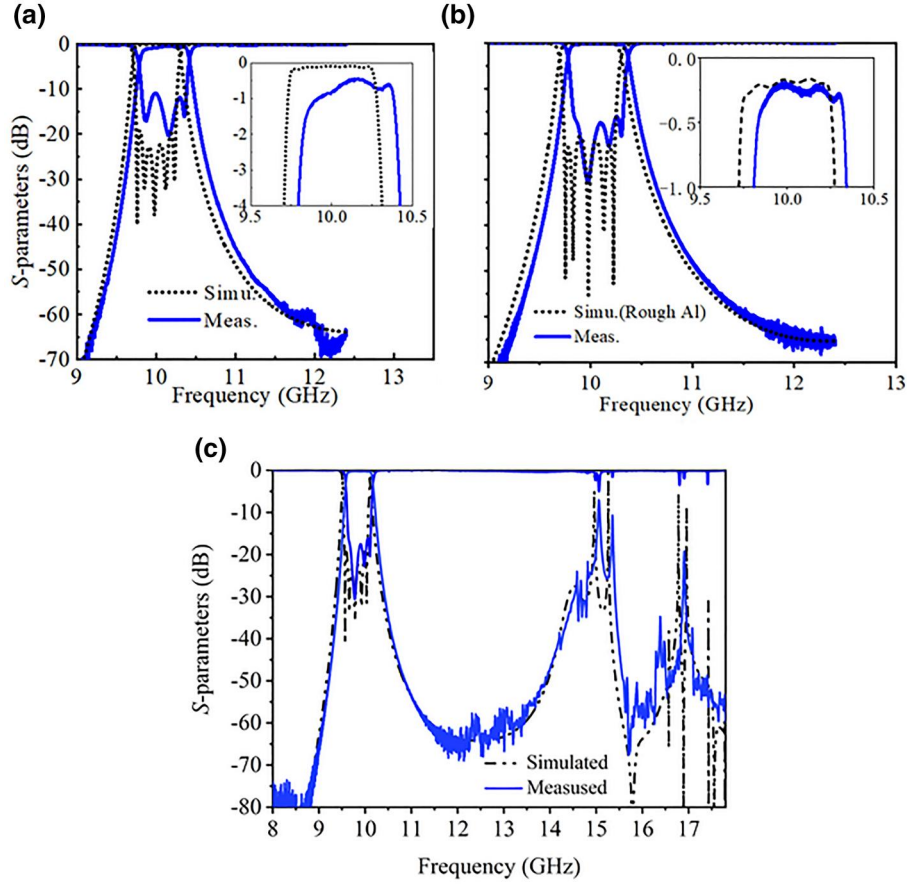


**FIGURE 18** Simulated and measured  $S$ -parameter responses of the Filter UD1. (a) X-band performance for the filter shown in Figure 17b; (b) X-band performance for the filter shown in Figure 17a; (c) The wideband (X-to-Ku-band) performance for the filter in Figure 17a. The effective electrical conductivity  $\sigma = 8 \times 10^6$  S/m was used in the simulation

where  $Q_{u-i}$  is the  $Q_u$  of the  $i$ th resonator corresponding to  $g_i$ . The  $g$  values for a fifth-order Chebyshev lowpass prototype filter are listed in Table 5. Intuitively, resonator 3 should be designed with the highest  $Q_u$  since the  $g_3$  is the largest, and the resonators 1 and 5 should with the lowest  $Q_u$  due to the smallest  $g_1$  and  $g_5$ . However, considered the fact that the sum ( $g_1 + g_5$ ) is apparently larger than  $g_3$ . Therefore, for the Filter UDS2, the highest- $Q_u$  resonators were assigned to the second and the fourth resonant nodes, while the lowest- $Q_u$  resonator was placed in the middle. The  $Q_u$  of the resonators for the Filter UDS2 are also included in Table 5. Using Equation (1), the insertion loss for this case was calculated to be 0.14 dB. Additionally, for a 20 dB RL, the corresponding passband ripple is about 0.04 dB. Hence, the estimated total IL of the Filter UDS2 is around 0.18 dB. Some critical design parameters for this filter are listed in Figure 19.

The filter was SLM-printed in the same tilted orientation as printed for the Filter UD1. Figure 20 shows the fabricated filter and Figure 21 shows the measured frequency responses after polishing. After polishing, the IL is around 0.2–0.3 dB. The filter exhibits a stopband (better than 34 dB) up to 18 GHz and at the same time, very little radiation was generated ( $S_{11} > -0.5$  dB for simulation and  $> -1$  dB for measurement).

**TABLE 5** Element values of the lowpass prototype filter for the Filter C and the EM-simulated  $Q_u$ s of the dimpled resonators

Resonator 1		Resonator 2		Resonator 3	
$g_1$	$Q_{u-1}$	$g_2$	$Q_{u-2}$	$g_3$	$Q_{u-3}$
0.9714	4503	1.3721	4945	1.8014	3840
Resonator 4		Resonator 5			
$g_4$	$Q_{u-4}$	$g_5$	$Q_{u-5}$	$g_0$	$g_6$
1.3721	5195	0.9714	4187	1	1

The  $Q_u$ s were evaluated for the dominant mode using the electrical conductivity of  $8 \times 10^6$  S/m for the aluminium alloy. The reference  $Q_u$ s for aluminium spherical and rectangular cavities are 5900 and 3190, respectively.

### 3.6 | More discussions on the radiation

Figure 22 shows a comparison in the simulated (using CST) total efficiencies of radiation for the Filters S3, DS1, UDS1 and UDS2. It can be noticed that for all the filters, the radiation from the slot in the passband is negligible but varies significantly in the stopband depending on the spurious mode suppression technique. The total efficiencies in the stopband are lower than  $-10$  dB for the Filters

UDS1 and UDS2, whereas it approaches 0 dB for the Filter S3 and DS1. This again validates a significant reduction in the stopband radiation by means of detuning the spurious resonances before slotting.

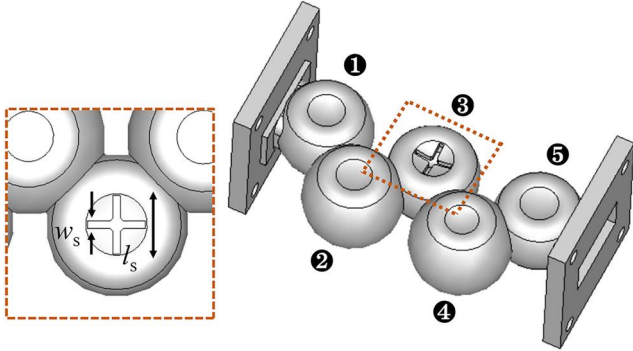


**FIGURE 19** A fabrication model of the Filter UDS2. Some critical dimensions are:  $r_{1-1} = 11.333$ ,  $d_1 = 4.5$ ,  $r_{1-2} = 12.022$ ,  $d_2 = 3.85$ ,  $r_{1-3} = 11.132$ ,  $d_3 = 6.2$ ,  $r_{1-4} = 12.215$ ,  $d_4 = 3.25$ ,  $r_{1-5} = 11.019$ ,  $d_5 = 5.1$ ,  $a_1 = 14.541$ ,  $d_{12} = 11.475$ ,  $d_{23} = 10.259$ ,  $d_{34} = 10.248$ ,  $d_{45} = 11.558$ ,  $l_s = 10.33$ ,  $w_s = 1.33$ ,  $r_2 = 15$  (for all the resonators)



**FIGURE 20** Photograph of the selective laser melting printed Filter UDS2

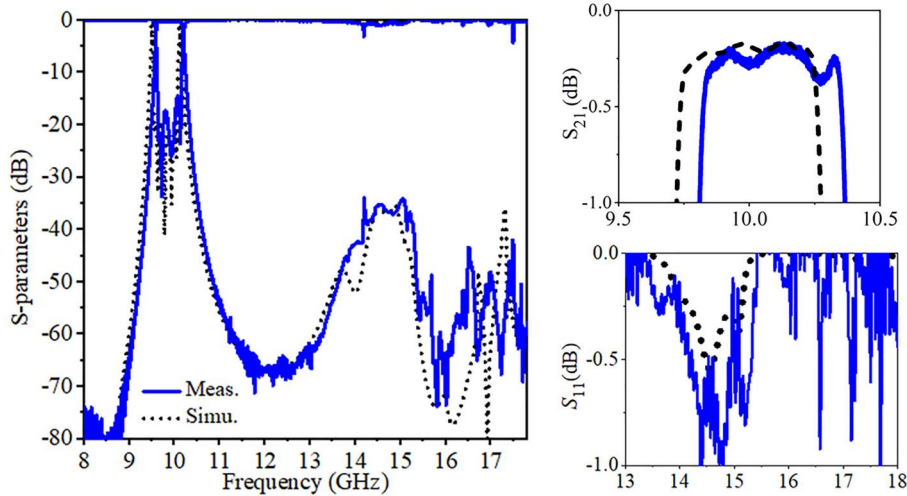


**FIGURE 21** Simulated and Measured  $S$ -parameter responses of the Filter UDS2

## 4 | CONCLUSION

This study proposes the technical solutions to extend the spurious-free stopband bandwidth for the waveguide BPF based on dimpled spherical resonators. This includes depression and slotting of the resonators and their combination. The X-band filters demonstrate excellent microwave performance in terms of small passband IL of 0.2–0.3 dB, RLs greater than 15 dB and frequency shifts less than 0.9% for the SLM filters. Wide spurious-free stopbands covering the entire Ku band with good stopband rejections have been realised.

The performances of the proposed filters are summarised in Table 6 and compared with some other work in terms of spurious suppression and loss. The technical highlights provided by this work include—(1) a significant extension of the spurious-free stopband bandwidth with a >34 dB rejection for the spherical-resonator-based waveguide filters, which

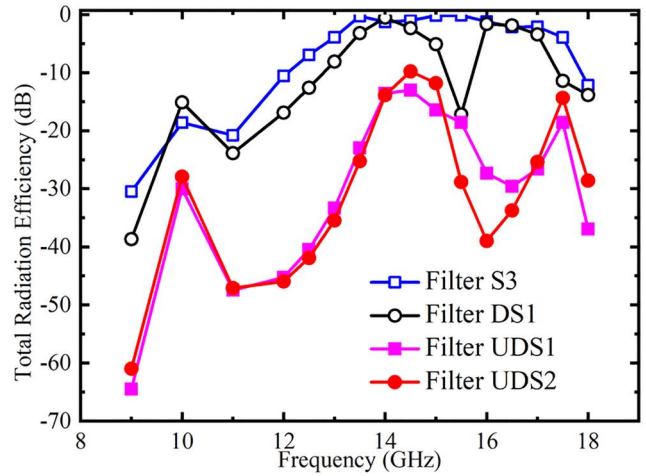


**FIGURE 22** Simulated total efficiency of the radiation for some typical filters

**TABLE 6** Comparison with the previously reported 3-D printed waveguide BPFs

References	$f_0$ (GHz)	FBW (%)	Filter Order	RL (dB)	IL (dB)	$\Delta f$ (%)	$f_1/f_0$	Spurious Suppression? <sup>a</sup>	Drawback	Types of Resonators	$Q_d/Q_{rec}$	AM Techniques
[15]	10	5	5	>20	0.11	0.05	1.32:1	—	—	Spherical	1.816	SLA + Cu plating
[16]	10	3	4	>18	0.24	<0.01	1.27:1	—	—	Dual mode spherical	—	—
[18]	3.5	4.57	8	>17	1.1/1.0	N/A	1.41:1	Yes (>40 dB)	—	Tri-mode spherical	1.37	N/A
[19]	6.545	1.8	3	>20	0.1	N/A	1.26:1	—	—	Tri-mode spherical	1.35	N/A
[20]	10	2.5	2	>20	0.9/0.47	N/A	N/A	—	—	Dual-mode ellipsoidal	1.8	SLA + Cu plating
[34]	12/12.5	1/1.92	4	>20	0.6/0.45	N/A	N/A	—	—	Dual-mode spherical	1.4	SLS + Cu plating
[21]	12.875	1.9	9	>20	0.55–0.8	0.12	1.55:1	Yes (>55 dB)	Tradeoff between Q/Rejection	Super-ellipsoid	1.13	SLM
[22]	12.875/14.125	1.94/1.77	3/5	>18	0.2	<0.2	>1.7:1	Yes (>55 dB)	—	—	—	—
[23]	10	1	3	>20	0.33/0.2	0.5/0.04	>1.7:1	Yes (>20 dB)	Radiative stopband	Slotted spherical	1.816	SLM/SLA+EP Cu
[24]	10	3	4	>15	0.9	<1	>1.6:1	Yes (>34 dB)	Low Q	Slotted hemispherical	1.04	SLM
[35]	11	0.91	5	>13–20	>2	>0.7	N/A	—	—	Shaped rectangular	1.16	SLM
Filter DS1	10	5	5	N/A	N/A	N/A	>1.8:1	Yes (>30 dB)	Radiative stopband	Slotted & equally dimpled	1.73	Simulation only
Filter UD1	10	5	5	>16	0.2–0.3	0.86	>1.52:1	Yes (>20 dB)	Tradeoff between Q/Rejection	Unequally dimpled	1.2–1.7	SLM
Filter UDS2	10	5	5	>15	0.2–0.3	0.9	>1.8:1	Yes (>34 dB)	Weakly radiative stopband	Unequally dimpled & slotted	1.2–1.7	SLM

*Note:*  $\Delta f$ , centre frequency shift;  $f_1/f_0$ , the frequency ratio of the measured first spurious passband to fundamental-mode passband frequency;  $Q_d/Q_{rec}$ , the  $Q_d$  ratio of the utilised resonator to the reference rectangular resonator.

Abbreviations: AM, additive manufacturing; FBW, Fractional bandwidth; IL, insertion loss; RL, return loss; SLM, selective laser melting.

<sup>a</sup>The out-of-band rejection performance is more dependent on the specified FBW.

experimentally validates the proposed concepts of shaping and slotting; (2) The trade-off between the  $Q_u$  and spurious-free bandwidth is alleviated and the resonators feature  $Q_u/Q_{Rec}$  from 1.2 to 1.7. (3) excellent passband performance of the filters in terms of >15 dB RLs, 0.2–0.3 dB ILs and small frequency shifts, which demonstrates high accuracy and reliability of the utilised AM process; (4) Designs are compatible with the RF and mechanical requirements, leading to ‘support-less’ and high-performance resonators. As compared with the previous works, not only the measured frequency ratio for the spurious-free stopband reaches >1.8:1, but also, the  $Q_u/Q_{Rec}$  is the largest.

## ACKNOWLEDGEMENT

The work was supported by the National Natural Science Foundation of China under Grant 62001367.

## CONFLICT OF INTEREST

The authors declare no conflict of interest.

## PERMISSION TO REPRODUCE MATERIALS FROM OTHER SOURCES

None.

## ORCID

Yang Yu  <https://orcid.org/0000-0002-4322-1415>

## REFERENCES

- Snyder, R.V., et al.: Present and future trends in filters and multiplexers. *IEEE Trans. Microw. Theor. Tech.* 63(10), 3324–3360 (2015)
- Yang, H., et al.: WR-3 waveguide bandpass filters fabricated using high precision CNC machining and SU-8 photoresist technology. *IEEE Trans. THz Sci. Technol.* 8(1), 100–107 (2018)
- Macchiarella, G., Tamiazzo, S.: Novel approach to the synthesis of microwave diplexers. *IEEE Trans. Microw. Theor. Tech.* 54, 4281–4290 (2006)
- Shang, X., et al.: Novel multiplexer topologies based on all-resonator structures. *IEEE Trans. Microw. Theor. Tech.* 61(11), 3838–3845 (2013)
- Zhao, P., Wu, K.L.: An iterative and analytical approach to optimal synthesis of a multiplexer with a star-junction. *IEEE Trans. Microw. Theor. Tech.* 62(12), 3362–3369 (2014)
- Chen, F.-C., et al.: X-band waveguide filtering antenna array with nonuniform feed structure. *IEEE Trans. Microw. Theor. Tech.* 65(12), 4843–4850 (2017)
- Mahmud, R.H., Lancaster, M.J.: High-gain and wide-bandwidth filtering planar antenna array-based solely on resonators. *IEEE Trans. Antenn. Propag.* 65(5), 2367–2375 (2017)
- Crestvolant, di, V.T., Iglesias, P.M., Lancaster, M.J.: Advanced butler matrices with integrated bandpass filter functions. *IEEE Trans. Microw. Theor. Tech.* 63(10), 3433–3444 (2015)
- Guo, C., et al.: A 135–150 GHz frequency tripler with waveguide filter matching. *IEEE Trans. Microw. Theor. Tech.* 66(10), 4608–4616 (2018)
- Guo, C., et al.: 290–310 GHz single sideband mixer with integrated waveguide filters. *IEEE Trans. THz Sci. Technol.* 8(4), 446–454 (2018)
- Palasantzas, G.: Surface roughness influence on the quality factor of high frequency nanoresonators. *J. Appl. Phys.* 103(4), 046106 (2008)
- Tischer, F.J.: Effect of surface roughness on surface resistance of plane copper surfaces at millimeter waves. *Proc. Inst. Electr. Eng.* 121(5), 333–336 (1974)
- Hilbert, D., Cohn-Vossen, S.: *Geometry and the Imagination*. American Mathematical Soc. p. 224. Providence (1999)
- Calignano, F., et al.: Overview on additive manufacturing technologies. *Proc. IEEE*, 105(4), 593–612 (2017)
- Guo, C., et al.: A 3-D printed lightweight X-band waveguide filter based on spherical resonators. *IEEE Microw. Wireless Compon. Lett.* 25(7), 442–444 (2015)
- Guo, C., et al.: A lightweight 3-D printed X-band bandpass filter based on spherical dual-mode resonators. *IEEE Microw. Wireless Compon. Lett.* 26(8), 568–570 (2016)
- Guo, C., et al.: Ceramic filled resin based 3D printed X-band dual-mode bandpass filter with enhanced thermal handling capability. *Electron. Lett.* 52(23), 1929–1931 (2016)
- Hendry, D.R., Abbosh, A.M.: Parallel multimode cavity filters with generalized frequency response. *IEEE Trans. Microw. Theor. Tech.* 67(5), 1844–1853 (2019)
- Gowrish, B., Koul, S.K., Mansour, R.R.: Transversal coupled triple-mode spherical resonator-based bandpass filters. *IEEE Microw. Wireless Compon. Lett.* 31(4), 369–372 (2021)
- López-Oliver, E., Tomassoni, C.: 3-D-printed dual-mode filter using an ellipsoidal cavity with asymmetric responses. *IEEE Microw. Wireless Compon. Lett.* 31(6), 670–673 (2021)
- Booth, P.A., Lluch, E.V.: Realising advanced waveguide bandpass filters using additive manufacturing. *IET Microw. Antenn. Propag.* 11(14), 1943–1948 (2017)
- Booth, P.A., Lluch, E.V.: Enhancing the performance of waveguide filters using additive manufacturing. *Proc. IEEE*, 105(4), 613–619 (2017)
- Zhang, F., et al.: 3-D printed slotted spherical resonator bandpass filters with spurious suppression. *IEEE Access*, 7, 128026–128034 (2019)
- Li, J., et al.: Monolithic 3D-printed slotted hemisphere resonator bandpass filter with extended spurious-free stopband. *Electron. Lett.* 55(6), 331–333 (2019)
- Guo, C., et al.: Shaping and slotting high-Q spherical resonators for suppression of higher order modes. In: 2019 IEEE MTT-S International Microwave Symposium (IMS), pp. 1205–1208. Boston (2019)
- Memarian, M., Mansour, R.R.: Quad-mode and dual-mode dielectric resonator filters. *IEEE Trans. Microw. Theor. Tech.* 57(12), 3418–3426 (2009)
- Tomassoni, C., Bastioli, S., Sorrentino, R.: Generalized TM dual-mode cavity filters. *IEEE Trans. Microw. Theor. Tech.* 59(12), 3338–3346 (2011)
- Hong, J.S., Lancaster, M.J.: *Microstrip Filters for RF/Microwave Applications*. Wiley, New York (2001)
- Howatson, A.M., Lund, P., Todd, J.D.: *Engineering Tables and Data*. Springer Science & Business Media, Dordrecht (1972)
- Zhou, J.G., He, Z.: Rapid pattern based powder sintering technique and related shrinkage control. *Mater. Des.* 19(5–6), 241–248 (1998)
- Zhu, H.H., Lu, L., Fuh, J.Y.H.: Study on shrinkage behaviour of direct laser sintering metallic powder. *Proc. Inst. Mech. Eng. B J. Eng. Manuf.* 220, 183–190 (2006)
- Singh, S., Sharma, V.S., Sachdeva, A.: Optimization and analysis of shrinkage in selective laser sintered polyamide parts. *Mater. Manuf. Process.* 27(6), 707–714 (2012)
- Salek, M., et al.: W-band waveguide bandpass filters fabricated by micro laser sintering. *IEEE Trans. Circ. Syst. Express Briefs.* 66(1), 61–65 (2019)
- Chen, Y., et al.: 3-D printed dual-band filter based on spherical dual-mode cavity. *IEEE Microw. Wireless Compon. Lett.* (2021). <https://doi.org/10.1109/LMWC.2021.3080430>
- Lorente, J.A., et al.: Single part microwave filters made from selective laser melting. In: *Proceedings of the European Microwave Conference*, Rome, pp. 1421–1424, Sept–Oct 2009

**How to cite this article:** Guo, C., et al.: Monolithic 3D printed waveguide filters with wide spurious-free stopbands using dimpled spherical resonators. *IET Microw. Antennas Propag.* 1–14 (2021). <https://doi.org/10.1049/mia2.12178>